TELKOMNIKA Indonesian Journal of Electrical Engineering
Vol. 14, No. 2, May 2015, pp. 250 ~ 265
DOI: 10.11591/telkomnika.v14i2.7361

Thermal Behavior of an Integrated Square Spiral Micro Coil

Y. Benhadda*[1], A. Hamid[1], T. Lebey[2], A. Allaoui[1], M. Derkaoui[1], R. Melati[1]
[1]University of Sciences and Technology of Oran (USTO- MB) 31000, Algeria
[2]University of Paul Sabatier, LAPLACE Laboratory, Toulouse, France
*Corresponding author, e-mail: benhadda_yamina@yahoo.fr

Abstract

We present in this paper a study on the thermal behavior of a square micro coil that will be integrated in a DC-DC micro converter. The first, we calculate the value of inductance. The second, we descript our micro coil; dimensioning, electrical model, and formula of loss. A buck micro converter schematic simulation coupled with ideal and integrated micro coil was presented. This conceptual model of the buck is best understood in terms of the relation between current and voltage of the inductor. Finely, we determinate a mathematical expression giving the evolution of temperatures in an integrated micro coil using the separation of variables method and a visualization of the thermal behavior is determined in 2D and 3D space dimension using the finite element method.

***Keywords**: micro coil, integrated, micro converter DC-DC, temperature*

Copyright © 2015 Institute of Advanced Engineering and Science. All rights reserved.

1. Introduction

In Power electronics, modeling of passive components constitute a particularly important issue. Indeed, the magnetic components, inductors and transformers are mainly used to transmit or store energy. The passive elements volume reduction leads to a mounted in operating frequency, but this increase in frequency causes an increase in losses. If the behavior of some components is relatively insensitive to temperature changes, it is not the same thing for magnetic components whose characteristics depend strongly on the temperature. The losses freed in the form of heat are become a major concern due to the reduction of trade with the outside surfaces and increasing the density of losses. Under these conditions, the inclusion of temperature and its influence on the magnetic and electrical characteristics of the component is essential. In this regard, several studies were conducted, first by the development of a compact model for the determination of the integrated component temperature [1], the study of the thermal model of integrated passive component based on the method node [2], the study of the thermal behavior in a bilayer materials by the method of separation of variables [3], the study of the thermal model of an integrated circuit by the method of Green [4] and finally the determination of the operating temperature of the integrated by a thermal analytical model passive component (Cauer model) [5]. The purpose of this work is the design and manufacturing of a micro coil for a micro converter. In operation, this reel is the seat of heat loss that we must quantified to ensure proper operation. Beyond a certain temperature, this micro coil may deteriorate and affect the operation of micro inverter. This led us to tackle the problem of thermal modeling of a square spiral coil micro plane. We have implemented the literature processes for the design of our micro coil and calculation of losses that are different from the heat. We have also developed mathematical models that allowed us to determine the thermal behavior of our component. The Solving of mathematical equations by the method of separation of variables [5] and the finite element method has allowed us to see the evolution of the temperature in the different parts that make up the micro coil in 2D and 3D.

2. Presentation of the Micro Converter

We have chosen a Buck micro converter continuous-continuous step-down (Figure 1) [6-9]. The micro coil to integrate will thus be dimensioned for this type of application. Input

Received January 20, 2015; Revised April 14, 2015; Accepted April 28, 2015

voltage, $V_{in} = 3Volt$. Output voltage, $V_{out} = 1.5Volt$. Maximum current $I_{L\max} = 0.65A$. Output power, $P_{out} = 0.6W$. Frequency of operation, $f = 1MHz$.

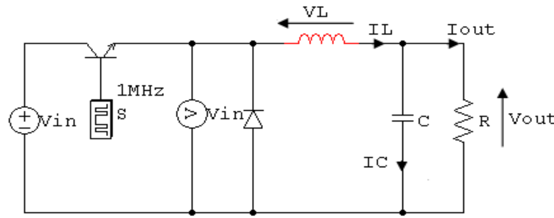

Figure 1. Buck converter

The average output current I_{out} is calculated by formula (1):

$$I_{out} = \frac{P_{out}}{V_{out}} \tag{1}$$

$I_{out} = 0.4A$, $I_{out} = L_L - I_c$, $I_c = 0$, $I_{out} = I_L$. The peak amplitude of the current through the micro coil is calculated by formula (2):

$$\Delta I_L = I_{L\max} - I_{L\min} \tag{2}$$

The average current I_L is expressed as follows (3):

$$I_L = \frac{I_{L\max} + I_{L\min}}{2} \tag{3}$$

Where,
$I_{L\min} = 2I_{out} - I_{L\max}$, $I_{L\min} = 0.016A$, $\Delta I_L = 0.96A$ and $\alpha = V_{out}/V_{in} = 0.5$.
The current which flows through the micro coil increases according to relation (4):

$$\Delta I_L = \frac{\alpha.(1-\alpha).V_{in}}{L.f} \tag{4}$$

We can calculate the value of the inductance L [9] according to relation (5):

$$L = \frac{\alpha.(1-\alpha).V_{in}}{\Delta I_l.f} \tag{5}$$

The maximum energy stored in the micro coil is given by relation (6):

$$W = \frac{1}{2} L I_{out}^2 \tag{6}$$

The volumetric energy density of the ferrite is given by the equation (7):

$$W_{v\max} = \frac{B_{\max}^2}{2\mu_0 \mu r} \tag{7}$$

$B_{\max}$: The maximum magnetic induction supported by the ferrite
μ_r: The relative permeability

μ_0 : The magnetic permeability of the free space

The volume of the ferrite is given by relation (8):

$$Vol = \frac{W}{W_{v\max}} \quad (8)$$

The ferrite's thickness is t_{Sub}=97µm, thus the volume will be $2100 \times 2100 \times 97 \mu m^3$.

3. Dimensioning of Integrated Inductor

The geometry parameters characterizing the integrated micro coil (Figure 2) are the number of turns ***n***, the width of the conductor ***w***, thickness of the conductor ***t***, the spacing between conductor ***s***, length of the conductor ***l***, the outer diameter $\boldsymbol{d_{out}}$ and input diameter $\boldsymbol{d_{in}}$.

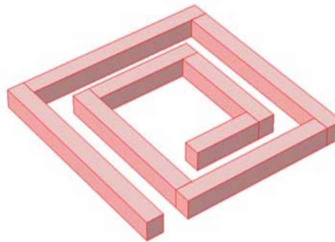

Figure 2. Geometry of integrated square spiral inductor

We find in the literature several formulas which allow us to calculate the number of turns n according to the value of inductance L, we chose the Weeler's [10-11] formula (9).

$$L_{mw} = K_1 \mu_0 \frac{n^2 d_{avg}}{1 + k_2 \rho} \quad (9)$$

Where, we define the average diameter as $d_{avg} = (d_{out} + d_{in})/2$ [12]. A_m the factor's form defined as $A_m = d_{out} - d_{in} / d_{out} + d_{in}$. The coefficients k_1 and k_2 are defined for each geometry. For a square micro coil spiral, k_1=2.34 and k_2=2.75.

The spacing between conductors is expressed as follows (10):

$$s = \frac{d_{out} + d_{in} - 2wn}{2(n-1)} \quad (10)$$

The length of the trace is expressed as follows (11)

$$l = 4n[d_{out} - (n-1)s - nw] - s \quad (11)$$

The skin thickness is defined as (12)

$$\delta = \sqrt{\frac{\rho}{\pi \mu f}} \quad (12)$$

Where ρ represent the resistivity of the conductor, $\rho_{Copper} = 1.7\ 10^{-8}\ \Omega.m$ and µ its magnetic permeability.So that the current flows in the entire conductor, it is necessary that one of the

following conditions is filled, $w \leq 2\delta$ or $t \leq 2\delta$, $\delta = 65.65\mu m$. Table 1 contains the specifications and the design results of the square spiral integrated micro coil.

Table 1. Design results of the spiral inductor

Parameter	Value
Inductance, L (μH)	1.15
Output diameter, d_{out} (mm)	2
Input diameter, d_{in} (mm)	0.4
Number of turns, n	2
Thickness of the conductor, t (μm)	40
Width of the conductor, w (μm)	120
Spacing between conductor, s (μm)	280
Length of the conductor, l (m)	0.0116

4. Electrical Model

The equivalent electrical model of the integrated micro coil [13-18] is shown in Figure 3.

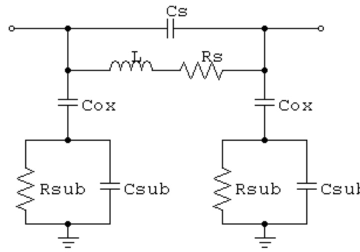

Figure 3. Equivalent electrical model

The series resistance R_s, can be approximated as (13):

$$R_s = \frac{\rho l}{wt} \tag{13}$$

The parasitic capacitive can be modeled as C_s (14):

$$C_s = tl\frac{\varepsilon_0 l}{s} \tag{14}$$

Where, ε_0 is the permittivity of free space, $\varepsilon_0 = 8.854187 10^{-12} Mm^{-1}$.

The substrate capacitance C_{sub} and resistance R_{sub} are approximately proportional to the area occupied by the integrated micro coil and can be expressed as (15), (16).

$$C_{sub} = \frac{1}{2}\varepsilon_0\varepsilon_r\frac{lw}{t_{sub}} \tag{15}$$

$$R_{sub} = 2\rho_{sub}\frac{t_{sub}}{lw} \tag{16}$$

C_{ox} oxide capacitance SiO_2 can be expressed as (17):

$$C_{ox} = lw\left(\frac{\varepsilon_0\varepsilon_{ox}}{t_{ox}}\right) \tag{17}$$

Where ε_r, ρ_{sub} represent respectively the relative permittivity and the resistivity of substrate and t_{ox} the oxide thickness. In our case, $\varepsilon_r = 10$, $\rho_{sub} = 45.10^{-6}\Omega m$ and $t_{ox} = 10\mu m$. The geometry of a square spiral integrated micro coil on substrate [19-20] is shown in Figure 4.

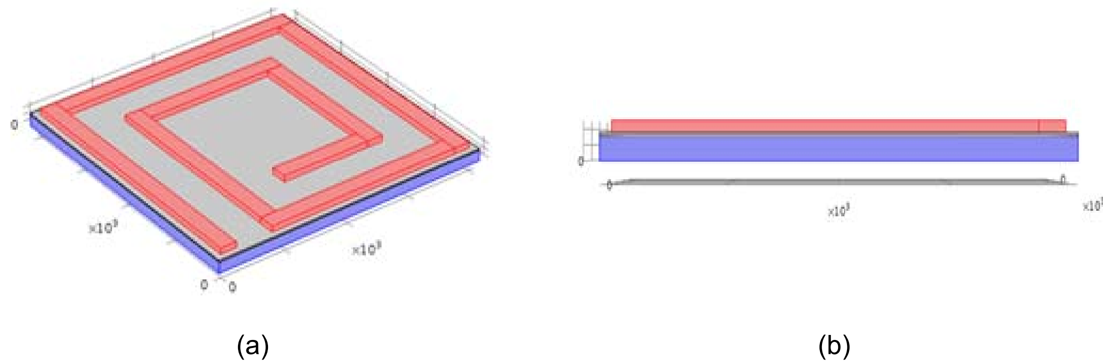

(a) (b)

Figure 4. Geometry of integrated square spiral inductor on substrate, (a) 3D view, (a) 2D view

The efficiency of integrated micro coil is calculated [21-22] according by relation (18):

$$Q = 2\pi \frac{\text{stocked energie}}{\text{dissipated energie}} \tag{18}$$

Table 2 presents electrical parameters of the integrated micro coil.

Table 2. Electricals parameters of the integrated square spiral inductor

Electricals parameters	Values
$R_s\,(\Omega)$	0.04
$R_{sub}\,(\Omega)$	0.006
$C_s\,(pF)$	0.014
$C_{ox}\,(pF)$	4.79
$C_{sub}\,(pF)$	0.76
Q	98.57

5. Loss Determination

The loss in the conductor [23-26] can be expressed as (19):

$$P_c = R_s.I^2 + R_{AC}.\Delta I_L^2 \tag{19}$$

Where, R_{AC} is the resistance at alternative current (20).

$$R_{AC} = \frac{\rho l}{\delta(1 - e^{-(t/\delta)})} \tag{20}$$

6. Simulation of the of the Micro Converter

In this simulation, the circuit of Figure 5 contains an ideal micro coil and the Figure 6 shows the waveform of the output voltage and current of the Buck micro converter. When the switch is closed, the voltage across the inductor is $V_L=V_{in}-V_{out}$. The current through the inductor

rises linearly. As the diode is reverse-biased by the voltage source, no current flows through it. When the switch is opened, the diode is forward biased. The voltage across the inductor is V_L= $-V_{out}$. The Current through inductor decreases.

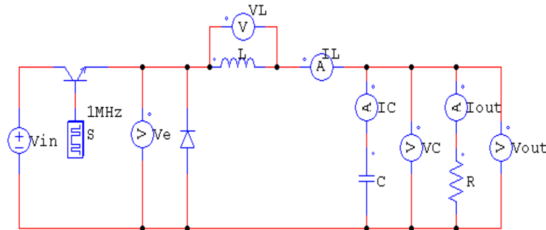

Figure 5. Schematic of buck micro converter coupled with ideal micro coil

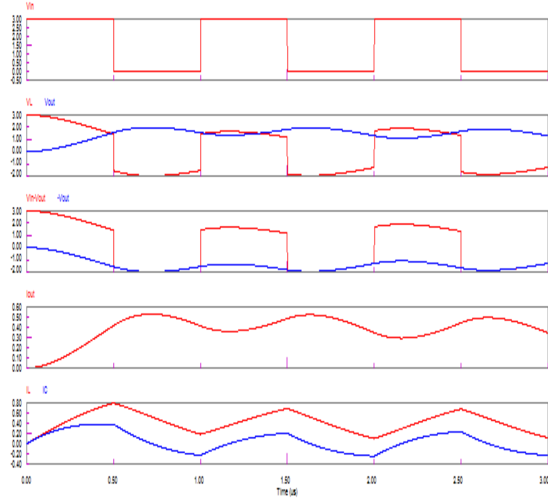

Figure 6. Waveforms of voltage and current of buck micro converter coupled with ideal micro coil

Figure 7 shows the schematic of micro converter simulated coupled with integrated micro coil. The simulated results are indicated in Figure 8. We observe the same result with ideal and reel inductor.

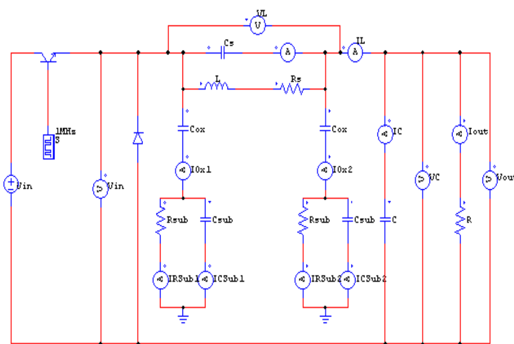

Figure 7. Schematic of buck micro converter coupled with integrated micro coil

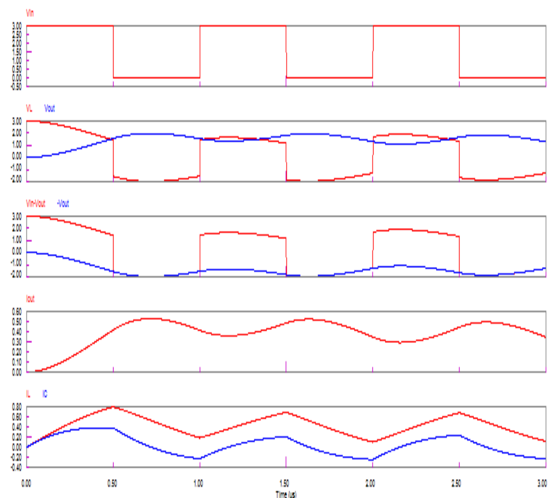

Figure 8. Waveforms of voltage and current of buck micro converter coupled with integrated micro coil

The results we obtained (Figure 6, Figure 8) were compared with those from the literature [27]. We notice the same evolutions therefore quite acceptable and in very good agreement.

7. Thermal Modeling of Integrated Inductor

In this section we will predict the evolution of the temperature in an integrated square spiral micro coil using:

a) Mathematical model based of the separation of variables method [28-30].
b) Visualization of the thermal behavior based of the finite element method [31-34].

We present an integrated micro coil in the air, with thickness L and heat source q (Figure 9). We consider also an integrated square spiral micro coil on substrate. k_1 , k_2 and k_3 be the thermal conductivities for the first layer in $0 \le y \le L_1$, second in $L_1 \le y \le L_2$ and third in $L_2 \le y \le L_3$. q is the heat source. Initially, the three layers are at temperature T_0. The boundary surface at y=0 is kept at temperature T_0 and the boundary at $y = L_1 + L_2 + L_3$, dissipate heat by convection with h constant (Figure 10).

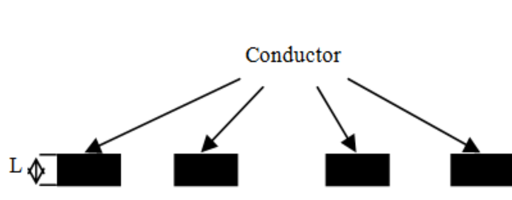

Figure 9. Transversal cup of an integrated micro coil in the air

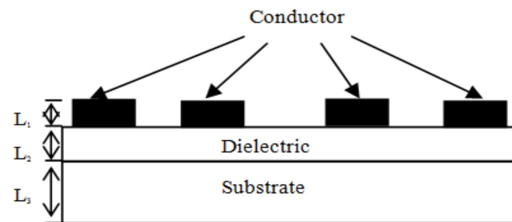

Figure 10. Transversal cup of an integrated micro coil on substrate

Our component consists of four domains. The domain of air surrounding our square spiral micro coil. The copper is the conductor material, the substrate is in NiFe, and the dielectric is in oxide SiO_2. The thermal characteristics of materials are shown in Table 3.

Table 3. Thermals Characteristics of the Materials

Element	Materiel	Characteristics
Conductor	Copper (Cu)	Thermal conductivity: k= 400W/m.K Heat capacity: C_p =385J/K.kg Density: r_{h0} =8700kg/m^3
Substrate	Ferrite (NiFe)	Thermal conductivity: k=30 W/m.K Heat capacity: C_p =700J/K.kg Density: r_{h0} =4000kg/m^3
Oxide	Silicon dioxide (SiO_2)	Thermal conductivity: k=1.4 W/m.K Heat capacity: C_p =350J/K.kg Density: r_{h0} =2000kg/m^3
Dielectric	Air	Thermal conductivity: k=0.03 W/m.K Heat capacity: C_p =1000J/K.kg Density: r_{h0} =1.2kg/m^3

7.1. Mathematical Model

The mathematical formulation of an integrated square spiral micro coil in the air is given as (21):

$$\frac{\partial^2 T}{\partial y^2} + \frac{1}{k} q = \frac{1}{\alpha} \frac{\partial T}{\partial t} \quad (21)$$

For solve this equation, we can determinate the solution analytical for homogeneous problem $T_h(y,t)$, and the solution of steady-state problem $T_s(y)$. The solution for the original problem (21) is determined from:

$$T(y,t) = T_h(y,t) + T_s(y) \tag{22}$$

To solve the homogeneous problem, we use the separation of variable of equation $T_h(y,t)$ into a space and time.

$$T_h(y,t) = \Gamma(t).Y(y) \tag{23}$$

The function $Y(y)$ become (24):

$$\frac{d^2 Y_1(x)}{dy^2} + \beta^2 Y(y) = 0 \tag{24}$$

The solution for $\Gamma(t)$ is given as (25):

$$\Gamma(t) = e^{-\alpha\beta^2 \mathrm{t}} \tag{25}$$

The solution for $T_h(y,t)$ is given as (26):

$$T_h(y,t) = \sum_{n=1}^{\infty} c_m e^{-\alpha\beta^2 \mathrm{t}}.Y(\beta_m, y) \tag{26}$$

For t=0, equation (26) becomes (27):

$$T_0 = \sum_{m=1}^{t} c_m.Y(\beta_m, y)^2 \tag{27}$$

With,

$$c_m = \frac{1}{N(\beta_m)}.\int_{y'=0}^{L} Y(\beta_m, y').T_0 dy' \tag{28}$$

$$N(\beta_m) = \int_0^L Y^2(\beta_m, y)dy \tag{29}$$

The analytical solution 1D for equation (21) is given as (30):

$$T_h(y,t) = \sum_{m=1}^{\infty} \frac{e^{-\beta_n^2.t}}{N(\beta_m)}.Y(\beta_m, y).\int_{y'=0}^{L} Y(\beta_m, y').T_0 dy' \tag{30}$$

With, $Y(\beta_m, y) = \sin \beta_m y$, $\frac{1}{N(\beta_m)} = \frac{2}{L}$ and $\sin \beta_m y = 0$. $\beta_m = m\pi/a$, $m = 1,2,3,\ldots$

$T_s(y)$ is the solution of the steady-state.

The mathematical formulation of an integrated square spiral micro coil on substrate is given as (31), for i=1, 2, 3.

$$\frac{\partial^2 T_i}{\partial y^2} + \frac{q}{k_i} = \frac{1}{\alpha_i}\frac{\partial T_i}{\partial t} \tag{31}$$

For solve this equation, we can determinate the solution analytical for homogeneous problem $\theta_i(y,t)$, and the solution of steady-state problem $T_i(y)$. We use the Green's function of heat conduction problems with heat source. The solution is determined from (32).

$$T_i(y,t) = \theta_i(y,t) + T_i(y) \tag{32}$$

The temperature boundary conditions are determined from (33).

$$\begin{aligned} &\theta_1 = 0, at: y = 0 \\ &\left.\begin{aligned} &\lambda_i \frac{\partial \theta_i}{\partial y} = \lambda_{i+1} \frac{\partial \theta_{i+1}}{\partial y} \\ &\theta_i = \theta_{i+1} \end{aligned}\right\}, \text{at interface}, i = 1,2 \\ &\lambda_3 \frac{\partial \theta_3}{\partial y} + h\theta_3, at: y = L_1 + L_2 + L_3 \end{aligned} \tag{33}$$

h represent the convective heat transfer coefficient. The initial condition is (34).

$$\theta_i(y,t) = T_0 \tag{34}$$

Where $\theta_i(y,t)$, is the temperature of the layer i.
For obtain the analytic solution of each layer, we use the solution by separation of variables (35)

$$\theta_i(y,t) = \Gamma_i(t).\Psi_i(y) \tag{35}$$

We determinate $\theta_i(y,t)$ with equation (36).

$$\theta_i(y,t) = \sum e^{-\beta_n^2 t}\left(A_{in} \sin \frac{\beta_n . y}{\sqrt{\alpha_i}} + B_{in} \cos \frac{\beta_n . y}{\sqrt{\alpha_i}}\right) C_n \tag{36}$$

The temperature distribution (36) must satisfy the initial condition (37).

$$T_0 = \sum_i C_n . \Psi_{in}(y) \tag{37}$$

By applying the operator: $\frac{\lambda_i}{\alpha_i} . \int_{y_i}^{y_{i+1}} \Psi_{ir}$ to the both sides of equation (37), we find (38).

$$\sum_{i=1}^{M} \frac{\lambda_i}{\alpha_i} \int_{y_i}^{y_{i+1}} \Psi_{ir}(y).T_0.dy = \sum_n C_n \left[\sum_{i=1}^{M} \frac{\lambda_i}{\alpha_i} . \int_{y_i}^{y_{i+1}} \Psi_{ir}.\Psi_{in} d\,y\right] \tag{38}$$

Where, M is the number of layer (M=3).

$$\sum_{i=1}^{M} \frac{\lambda_i}{\alpha_i} . \int_{y_i}^{y_{i+1}} \Psi_{in}.\Psi_{ir}\, d\,y = \begin{cases} 0 & n \neq r \\ N_n & n = r \end{cases} \tag{39}$$

The N_n and C_n expressions are defined, respectively, as follows (40), (41).

$$N_n = \sum_{j=1}^{M} \frac{\lambda_i}{\alpha_j} . \int_{y_i}^{y_{i+1}} \Psi_{jn}^{\ 2} \, dy \tag{40}$$

$$C_n = \frac{1}{N_n} . \sum_{i=1}^{M} \frac{\lambda_i}{\alpha_i} . \int_{y_i}^{y_{i+1}} \Psi_{in} \ .T_0 .dy \tag{41}$$

Finally, the temperature expression is now (42).

$$\theta_i(y,t) = \sum_{i=1}^{n} \frac{e^{-\beta_n^{\ 2}.t}}{N_n} . \Psi_{in} . \sum_{i=1}^{M} \frac{\lambda_i}{\alpha_i} . \int_{y_i}^{y_{i+1}} \Psi_{in} \ .T_0 .d\ y \tag{42}$$

We replace Ψ_{in} by its expression, we will have (43).

$$\theta_i(y,t) = \sum_{n=1}^{\infty} \frac{1}{N_n} e^{-\beta_n^{\ 2}.t} (A_{in} \sin \frac{\beta_n . y}{\sqrt{\alpha_i}} + B_{in} \cos \frac{\beta_n . y}{\sqrt{\alpha_i}}) G \tag{43}$$

The solution $T_s(y)$ is determined from (44).

$$T_s(y) = \phi_i(y).T_0 + \Psi_i(y).T_0 \tag{44}$$

The functions $\phi_i(y)$ and $\Psi_i(y)$ are the solutions of the steady-state. The solution of the heat equation with heat source is given by Green's function $G_{ij}(y,t|x',\tau)$ [35-41](45).

$$T_i(y,t) = \sum_{j=1}^{M} \left\{ \begin{array}{l} \int_{y_j}^{y_{j+1}} y' \left| G_{ij}\, y,t \middle| y',\tau) \right|_{\tau=0} T_0 dy' + \int_{\tau=0}^{t} d\tau . \\ \int_{y_j}^{y_{i+1}} y' G_{ij}(y,t|y',\tau) \left[\frac{\alpha_j}{k_j} q \right] dy' \end{array} \right\} \tag{45}$$

7.2. Results

In this section, we present the temperature profile of our integrated micro coil. These results relate the variation and temperature distribution in each layer, conductor, dielectric and substrate. Figure 11 shows the temperature profile in an integrated micro coil on the air.

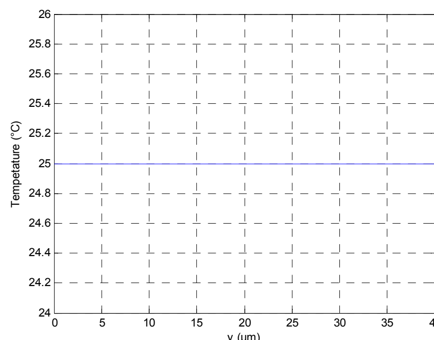

Figure 11. Temperature profile in an integrated inductor on the air

In Figure 12(a), (b) and (c), we observe the evolution of temperature in an integrated micro coil on substrate in a conductor, dielectric and in a substrate, respectively. The

temperature distribution increase in the copper and it decreases in the silicon oxide layers, and the substrate. Our results were compared with those from the literature [5]. We notice the same evolutions therefore quite acceptable and in very good agreement.

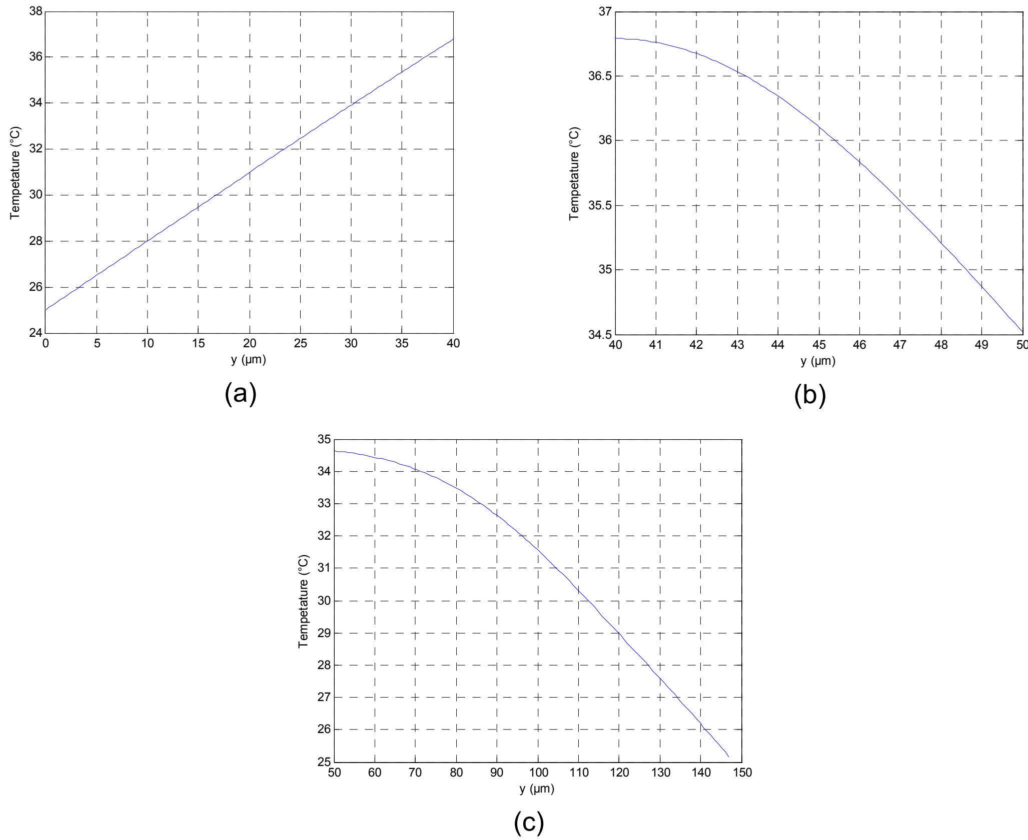

Figure 12. Evolution of temperature in an integrated micro coil on substrate in a, (a) conductor, (b) dielectric and (c) substrate

7.3. Visualization of the Thermal Behavior

In this section, we present the temperature distribution in our integrated micro coil, based on the finite element method [42].

Geometry of this study is created in 2D and 3D space dimension. This distribution is obtained by solving the equation (46) of heat taking into account certain boundary conditions.

$$\rho.C_p \frac{\partial T}{\partial t} - \nabla(k\nabla T) = q \tag{46}$$

Figure 13, (a) and (b) shows the geometry and mesh of micro coil in the air.

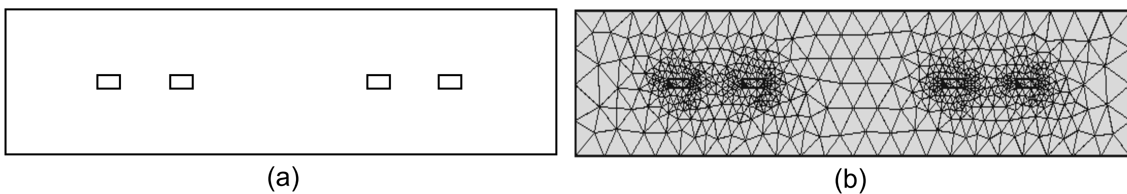

Figure 13. Micro coil in the air, (a) geometry, (b) mesh

Figure 14, (a) and (b) shows the geometry and mesh of micro coil on substrate.

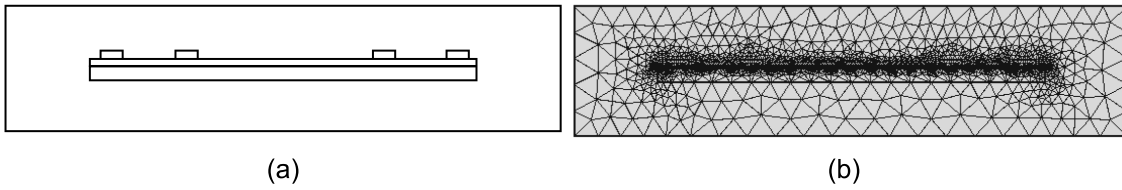

(a) (b)

Figure 14. Micro coil on substrate, (a) geometry, (b) mesh

Figure 15 presents the temperature distribution of integrated micro coil in the air, (a) on surface, (b) on contour. The maximum of the temperature is from 25°C.

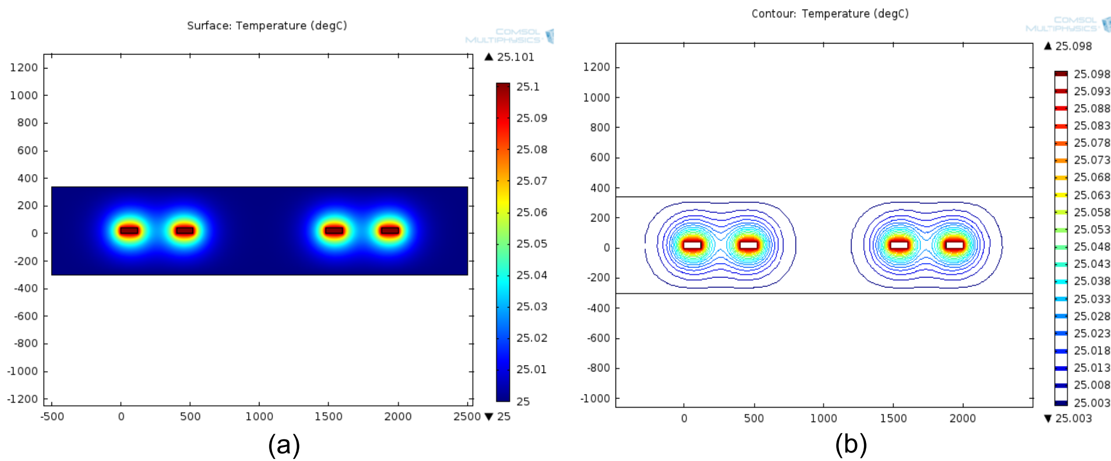

(a) (b)

Figure 15. Temperature distribution of integrated micro coil in the air, (a) on surface, (b) on contour

Figure 16 shows the total heat flux distribution of integrated micro coil in the air, (a) on surface, (b) on contour.

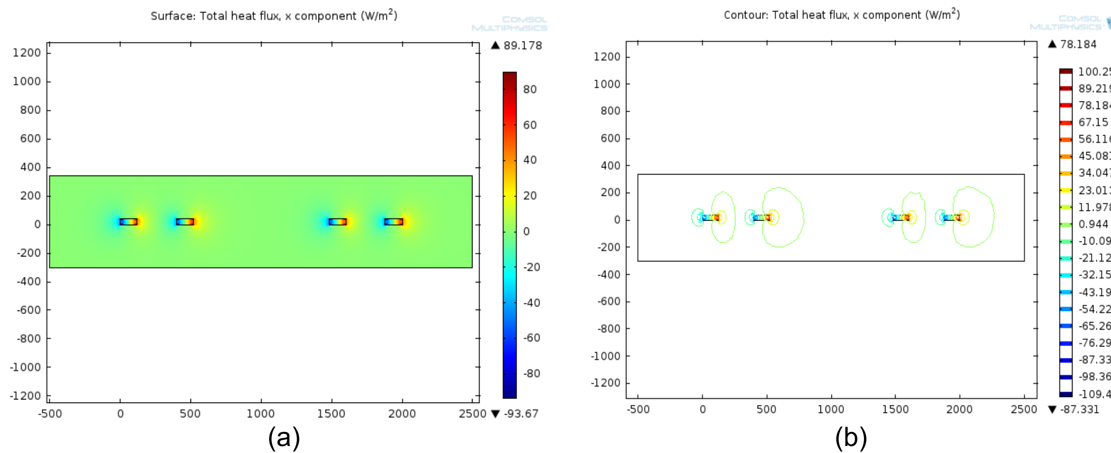

(a) (b)

Figure 16. Total heat flux distribution of integrated micro coil in the air, (a) on surface, (b) on contour

In Figure 17, we observe the temperature distribution of micro coil on substrate, (a) on surface, (b) on contour. We note that the maximum of the temperature is from 37 °C.

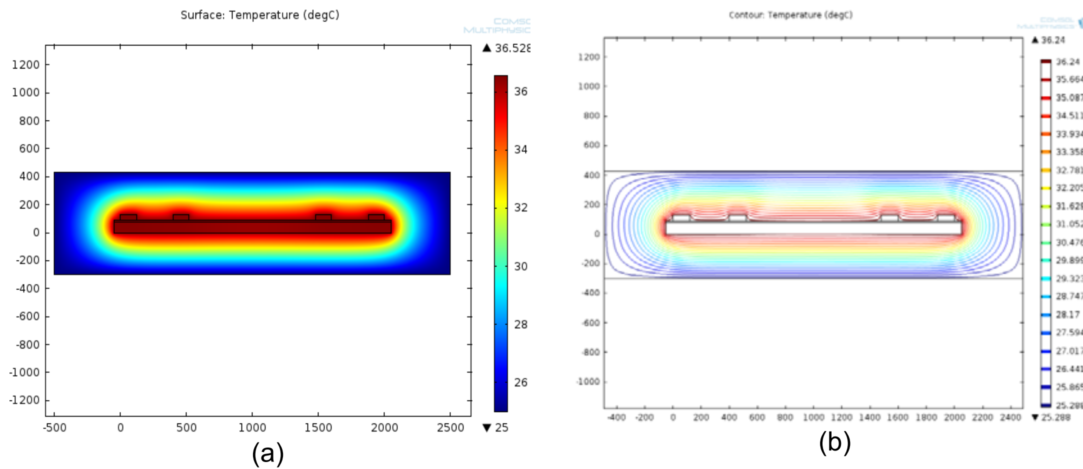

Figure 17. Temperature distribution of integrated micro coil on substrate, (a) on surface, (b) on contour

In Figure 18, we observe total heat flux distribution of micro coil on substrate, (a) on surface, (b) on contour.

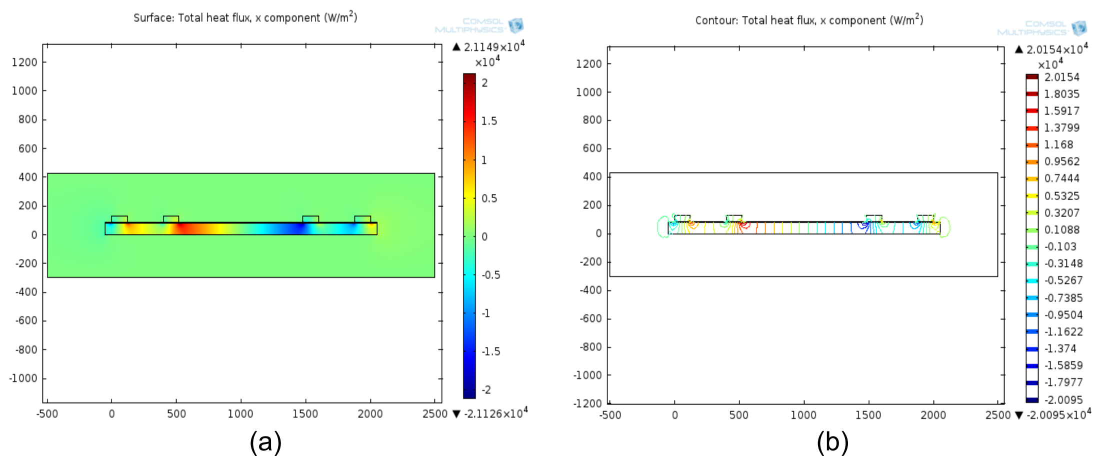

Figure 18. Total heat flux distribution of integrated micro coil on substrate, (a) on surface, (b) on contour

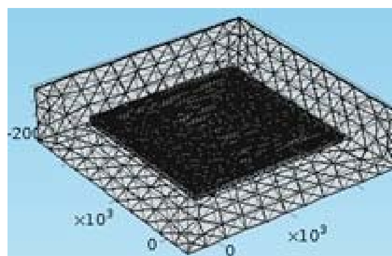

Figure 19. 3D mesh of micro coil on substrate

(a) (b)

(c) (d)

(e)

Figure 20. Temperature distribution in the micro coil on substrate, (a) on isosurface, (b) on the upper surface, (c) on surface, (d) on scile, (e) on contour

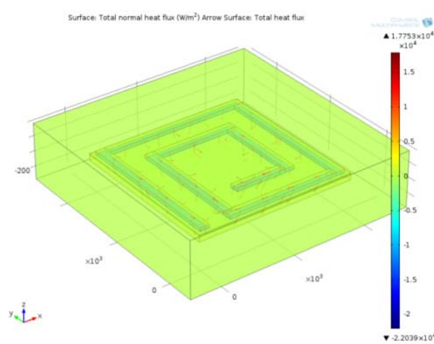

Figure 21. Total heat flux distribution in the micro coil on substrate

In Figure 19, we observe 3D mesh of integrated micro coil on substrate.

In Figure 20, we observe the temperature distribution in the micro coil on substrate, (a) on isosurface, (b) on the upper surface, (c) on surface, (d) on scile, (e) on contour. We see from these figures that the temperature attained is from 37 °C. Our results were compared with those from the literature [5]. We notice the same evolutions therefore quite acceptable and in very good agreement.

In Figure 21, we observe the total heat flux distribution in the micro coil on substrate.

8. Conclusion

Thermal modeling of an integrated square spiral micro coil is a very important point in microelectronic system. In this study, the temperature distribution in the different layers of integrated micro coil can be determined as a function of position and time from the heat conduction equation using two methods. The first is a mathematical model based of the separation of variables. The second nomad element finite is presented for a good visualization of thermal behavior in our component. Our geometry is created in 2D and 3D space dimension. It is found that the temperature in micro coil increase considerably when we add substrate. It has been demonstrated that the dependences of the heat source and loss, can be simulated the thermal behavior.

References

[1] S M'rad. Application de la représentation diffusive à la modélisation thermique compacte. Institut national des sciences appliqués. 2008.

[2] K Lai-Dac. Contribution à l'optimisation du dimensionnement de composants passifs intégrés pour l'électronique de puissance. Université Grenoble. 2010.

[3] M H Belghazi. Modélisation analytique du transfert instationnaire de la chaleur dans un matériau bicouche en contact imparfait et soumis à une source de chaleur en mouvement. Université de Limoges. 2008.

[4] Y Zhan, B Goplen, SS Sapatnekar. Electrothermal Analysis and Optimization Techniques for Nanoscale Integrated Circuits. *IEEE*. 2006: 219-222.

[5] A Allaoui, A Hamid, P Spiterri, V bley, T Lebey. Thermal modeling of an integrated inductor in a micro-converter. *Journal of Low Power Electronics.* 2015; 11(1): 63-73.

[6] Jeya Selvan Renius A, Vinoth Kumar K, Arnold Fredderics, Raja Guru, Sree Lakshmi Nair. Modelling of Variable Frequency Synchronous Buck Converter. *International Journal of Power Electronics and Drive System (IJPEDS)*. 2014; 5(2): 237-243.

[7] R Melati, A Hamid, T Lebey. *Modeling and Dimensioning of a Planar Inductor for a Monolithic Integration*. APPEEC'11 Proceedings of the 2011 Asia-Pacific Power and Energy Engineering Conference, IEEE. 2011.

[8] R Melati, A Hamid, T Lebey, M Derkaoui. Design of a New Electrical Model of a Ferromagnetic Planar Inductor for its Integration in a Micro converter. *Mathematical and Computer Modelling*. 2013; 57: 200-227.

[9] L Xian, Y Wang *An. Advanced-Time-Sharing Switching Strategy for Multiple-Input Buck Converters*. IEEE International Conference. 2014: 1067-1071.

[10] SS Mohan, MdM Hershenson, SP Boyd, TH Lee. Simple Accurate Expressions for Planar Spiral Inductances. *IEEE Journal of solid-state circuits.* 1999; 34(10): 1419-1424.

[11] N Arbabi, M Najmabadi, V Devabhaktuni, M Yagoub. A New SQP Based Space-Mapping Algorithm for on-chip spiral inductor optimization. *IEEE.* 2007: 99-102.

[12] ED Gadjeva, VP Durev, MH Hristov, DI Pukneva. *Optimization of geometric parameters of spiral Inductors Using Genetic Algorithms*. International Conference. 2006: 514-517.

[13] Rui Guo, Cong Wang, Tao Li. *Optimum Design of Coupling Inductors for Magnetic Integration in Three-Phase Interleaving Buck DC/DC Converter*. 8th IEEE Conference. 2013: 1029-1033.

[14] CP Yue, CRyu, J Lau, TH Lee, SS Wong. A Physical Model for Planar Spiral Inductors on Silicon. *IEEE*. 1996: 154-158.

[15] H Fuketa, Shinozuka, K Ishida, M Takamiya, T Sakurai. *On-Chip Buck Converter with Spiral Ferrite Inductor and Reducing IR Drop in 3D Stacked Integration*. IEEE Power Electronics Conference. 2014: 2228-2231.

[16] M Kaluża, A Napieralski. Frequency Sampling Approach to the Problem of Silicon Integrated Spiral Inductors Modeling. *Bulletin of the polish academy of sciences technical sciences.* 2008; 56(1): 21-27.

[17] A Tasic, WA Serdijn. Effects of Substrate on Phase-Noise of Bipolar Voltage-Controlled Oscillators. *IEEE*. 2002: 819-822.

[18] CP Yue, SS Wong. Physical Modeling of Spiral Inductors on Silicon. *IEEE Transactions on Electron Devices.* 2000; 47(3): 560-568.
[19] MK Yapici, JM Hong, J Zou, K Balareddy. *Post-CMOS On-Chip Integration of 3D MEMS Inductors Using a Novel Chip Embedding Technique*. The 17th IEEE International Conference. 2013: 128-131.
[20] C Liu, H Chang, K Li, C Lin, C Hsu, T Lin, H Chou, H Huang, H Liao. *Adaptable and Integrated Packaging Platform for MEMS-Based Combo Sensors Utilizing Innovative Wafer-Level Packaging Technologies*. IEEE Electronic Components & Technology Conference. 2013: 1675-1681.
[21] CP Yue, SS Wong. On-Chip Spiral Inductors with Patterned Ground Shields for Si-Based RFIC's. *IEEE Journal of Solid-State Circuits.* 1998; 33(5): 743-752.
[22] TG Imre, U Viscarret, IE Otadui, A Rufer. Transient Thermal Model of a Medium Frequency Power Transformer. *IEEE*. 2008: 1033-1038.
[23] C Wang, H Liao, C Li, R Huang, W Wong, X Zhang, Y Wang. A Wideband Predictive. Double-π Equivalent-Circuit Model for On-Chip Spiral Inductors. *IEEE Transactions on Electron Devices.* 2009; 56(4): 609-619.
[24] SY Lee, L Zhao, JT Strydom, WG Odendaal, D Van Wyk. Thermal Analysis for Series LC Integrated Passive Resonant Module Based on Finite-Element Modeling. *IEEE*. 2002; 1009-1014.
[25] R Petkov. Optimum Design of a High-Power, High-Frequency Transformer. *IEEE Transactions on Power Electronics*. 1996; 11(1): 33-42.
[26] P Viarouge, JC Fagundes, E Tourkhani, H Le-Huy. Comportement Thermique et Conception des Composants Magnétiques dans les Convertisseurs Statiques de Fréquence Elevée. *IEEE*. 1995: 582-585.
[27] R Melati. Conception d'un nouveau modele d'inductance integree. Université des sciences et de technologie; 2013.
[28] Bejan A. Heat Transfer. Second edition. Wiley. 1993.
[29] RI Hickson, SI Barry, GN Mercer. Critical Times in Multilayer Diffusion. *Part 1: Exact solutions. Preprint submitted to International Journal of Heat and Mass Transfer*. 2009.
[30] Y Tamene, C Bougriou, R Bessaïh. Thermal Behaviour of a Multilayer Media in Transient Regime. *Revue des Energies Renouvelables.* 2007; 10(3): 397-405.
[31] P Sharma, M Mehta. Analysis of RF MEMS Square Spiral Inductor. *International Journal of Scientific & Engineering Research*. 2012; 3(2): 1-4.
[32] Q Qian, Y Liu. *Reliability Analysis of Next Generation Wafer Level Chip Scale*. IEEE 14th International Conference on Thermal Mechanical and Multi-physics Simulation and Experiments in Microelectronics and Microsystems. 2013: 1-7.
[33] MC Hsieh. Finite Element Analyses for Critical Designs of Low-Cost Wafer-Level Chip Scale Packages. *IEEE Transactions on Components, Packaging and Manufacturing Technology.* 2014; 4(3): 451-458.
[34] L Ying, H Chunyue, Z Xin, L Tianming, G Guangkuo, X Guoji, T Wenliang. *Influence of Compliant Layer Thickness on Stress and Strain of Solder Joints in Wafer Level Chip Scale Package under Thermal Cycle*. IEEE 15th International Conference on Electronics Packaging Technology. 2014: 577-582.
[35] I MS, MRK Akanda. 3D Temperature Distribution of SiC MESFET Using Green's Function. *Electrical and Computer Engineering, IEEE*. 2010: 13-16.
[36] M Janicki, A Napieralski. Application of Green's Functions for Thermal Analysis of Electronic Circuits. *IEEE.* 2005: 435-438.
[37] B Wang, P Mazumder. Accelerated Chip-Level Thermal Analysis Using Multilayer Green's Function. *IEEE Transactions on Computer-Aided Design of Integrated Circuits and Systems*. 2007; 26(2): 325-344.
[38] Y Zhan, SS Sapatnekar. High-Efficiency Green Function-Based Thermal Simulation Algorithms. *IEEE Transactions on Computer-Aided Design of Integrated Circuits and Systems.* 2007; 26(9): 1661-1675.
[39] SH Pan, N Chang, T Hitomi. 3D-IC Dynamic Thermal Analysis with Hierarchical and Configurable Chip Thermal Model. *IEEE*. 2013.
[40] BJ Tsai, CC Chen, G Chen, B Goplen, H Qian, Y Zhan, S Kang, MDF Wong, SS Sapatnekar. Temperature-Aware Placement for SOCs. *IEEE*. 2006; 94(8): 1502-1518.
[41] D Oh, CCP Chen, YH Hu. 3DFFT: *Thermal Analysis of Non-Homogeneous IC Using 3D FFT Green Function Method*. IEEE Proceedings of the 8th International Symposium on Quality Electronic Design. 2007.
[42] M Derkaoui, A Hamid, T Lebey, R Melati. Design and Modeling of an Integrated MicroTransformer in a Flyback Converter. *TELKOMNIKA*. 2013; 11(4): 669-682.